

Strain hardening behavior of a friction stir welded magnesium alloy

N. Afrin,^a D.L. Chen,^{a,*} X. Cao^b and M. Jahazi^b

^aDepartment of Mechanical and Industrial Engineering, Ryerson University, 350 Victoria Street, Toronto, Ontario M5B 2K3, Canada

^bAerospace Manufacturing Technology Centre, Institute for Aerospace Research, National Research Council Canada, 5145 Decelles Avenue, Montreal, Quebec H3T 2B2, Canada

Received 25 June 2007; revised 29 July 2007; accepted 1 August 2007

Available online 4 September 2007

The work hardening properties of a friction stir welded (FSWed) magnesium alloy were evaluated using two modified equations of hardening capacity and strain hardening exponent where the elastic deformation stage was excluded. Kocks–Mecking type plots were used to show different stages of strain hardening. The hardening capacity of the FSWed samples was observed to be about twice that of the base alloy, while the strain hardening exponent of the FSWed samples was nearly threefold higher than that of the base alloy.

Crown Copyright © 2007 Published by Elsevier Ltd. on behalf of Acta Materialia Inc. All rights reserved.

Keywords: Friction stir welding; Magnesium alloys; Mechanical properties; Plastic deformation; Work hardening

In the aerospace and automotive industries the use of magnesium alloys are increasing due to their high strength-to-weight ratio. Welding is one of key joining techniques in the manufacturing of engineering components. The conventional welding techniques often produce some defects in the fusion zone or heat-affected zone [1]. Friction stir welding (FSW), a novel solid-state joining technique [2], is an enabling technology for joining Mg alloys which are difficult to weld by conventional techniques [3,4]. Several studies have demonstrated a good potential of this technique for joining Mg alloys [4–9].

Strain hardening behavior is one of the important considerations in the evaluation of plastic deformation of materials [10,11], thus numerous investigations have been conducted. Kovács et al. [12] reported that the strain hardening parameter was highly influenced by grain size at moderate strains, but was independent of the grain size at higher strains in pure aluminum. Johnston and Feltner [13] showed that the major source of grain boundary strengthening of polycrystals was due to the enhanced strain hardening effect that stems from the dynamic imbalance in the rates of plastic flow on both sides of individual grain boundaries. Strain hardening of ultrafine-grained copper with nanoscale twins was recently studied by Chen and Lu [11]. So far only limited studies are reported on the strain hardening

behavior of Mg alloys [14–16], and no work on the strain hardening of the FSWed Mg alloy is seen in the open literature. The aim of the present investigation was, therefore, to study the effects of FSW on the strain hardening behavior of AZ31B Mg alloy.

AZ31B-H24 Mg alloy, with a thickness of 4.95 mm and a composition of 2.5–3.5% Al, 0.7–1.3% Zn, 0.20–1.0% Mn and the balance Mg, was selected. FSW was carried out perpendicular to the rolling direction using an MTS FSW system. Two welding speeds, 2 and 4 mm s^{−1}, indicated by samples IV and VI, respectively, were used at a pin tool rotational speed of 1000 rpm. Microstructures of the FSWed joints cut perpendicular to the welding direction were examined using light microscopy and scanning electron microscopy. Tensile tests of the samples prepared according to ASTM E8 standards were performed using a computerized tensile testing machine at room temperature and varying strain rates from 7×10^{-6} to 3×10^{-2} s^{−1}.

Figure 1 shows a typical example of the true stress vs. true strain curves of the base alloy, FSWed samples VI and IV tested at a strain rate of 6.7×10^{-5} s^{−1}. Flow stresses were higher in the base alloy than those in the FSWed samples. Microstructural examinations of the base alloy showed smaller elongated grains of average size of $\sim 5 \mu\text{m}$, whereas the FSWed samples demonstrated larger recrystallized/equiaxed grains of $\sim 9 \mu\text{m}$ in the stir zone (SZ) [17]. The base alloy in H24 condition contained a large number of dislocations and required a higher applied stress to deform the material.

* Corresponding author. Tel.: +1 416 979 5000x6487; fax: +1 416 979 5265; e-mail: dchen@ryerson.ca

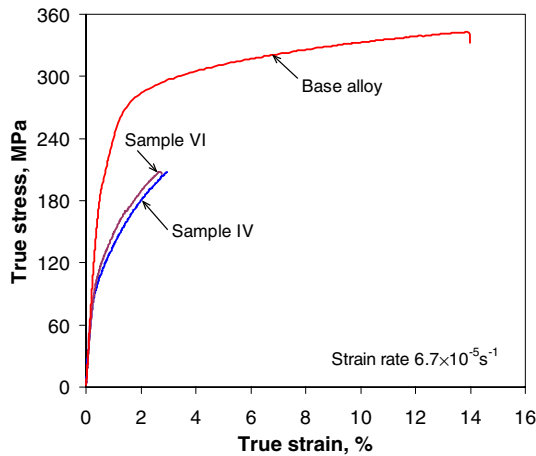


Figure 1. Typical true stress vs. true strain curves of AZ31B-H24 base alloy, FSWed samples IV and VI tested at a strain rate of $6.7 \times 10^{-5} \text{ s}^{-1}$.

The FSWed samples in the annealing-like condition had fewer dislocations, and thus needed a lower stress to start the deformation.

Figure 2 shows a Kocks–Mecking type plot of strain hardening rate $\theta (=d\sigma/d\varepsilon)$ vs. net flow stress $(\sigma - \sigma_y)$ at a strain rate of $6.7 \times 10^{-5} \text{ s}^{-1}$. While θ decreased continuously in the FSWed samples, a high initial θ value that remained at an almost constant 11,000 MPa until the net flow stress reached nearly 30 MPa was seen in the base alloy, indicating an initially linear strain hardening of stage II behavior. This can also be seen in Figure 1. Then θ decreased rapidly and linearly, exhibiting stage III hardening behavior [18,19]. When the net flow stress exceeded ~ 70 MPa, θ became small and hardening stage IV [18,19] occurred in the base alloy. The FSWed samples showed an initial θ value of approximately 8000 MPa. However, no stage II hardening was observed, and stage III hardening, characterized by a linear decrease in θ , appeared immediately after yielding. The slope was slightly smaller in the FSWed samples IV (2 mm s^{-1} welding speed) than in samples VI (4 mm s^{-1} welding speed).

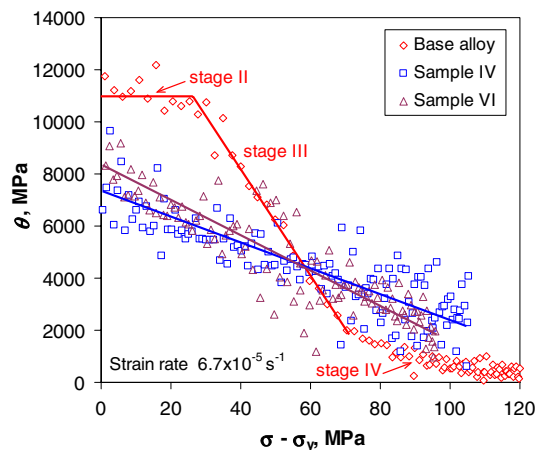


Figure 2. Strain hardening rate (θ) as a function of net flow stress $(\sigma - \sigma_y)$ of the base alloy, FSWed samples IV and VI tested at a strain rate of $6.7 \times 10^{-5} \text{ s}^{-1}$.

The hardening capacity, H_c , of a material may be considered as a ratio of the ultimate tensile strength (UTS), σ_{UTS} , to the yield strength (YS), σ_y [18]. In the present study the hardening capacity is re-defined as the following normalized parameter,

$$H_c = \frac{\sigma_{\text{UTS}} - \sigma_y}{\sigma_y} = \frac{\sigma_{\text{UTS}}}{\sigma_y} - 1 \quad (1)$$

Table 1 shows the hardening capacity of the base alloy and FSWed samples tested at different strain rates. While the YS and initial θ value were lower, the hardening capacity was higher in the FSWed samples than in the base alloy. The hardening capacity of a material is related to its yield strength, which is further associated with the grain size according to the Hall–Petch relationship [10,20,21]. An increase in the grain size would decrease the YS and increase the hardening capacity. A decrease in the grain size reduces the difference of the flow resistance between the grain boundary and interior, which in turn reduces the hardening capacity [18]. Another factor was related to the material condition. The base alloy was in the partially hardened H24 condition, whereas the FSWed samples exhibited an annealing-like condition and thus higher hardening capacity.

The flow stress of a material in the uniform plastic deformation region is commonly expressed by the Hollomon relationship [21–24]:

$$\sigma = K\varepsilon^n \quad (2)$$

where n is the strain (or work) hardening exponent, K is the strength coefficient, σ is the true stress and ε is the true strain. To quantify better the strain hardening response, Chen and Lu [11] fitted their tensile curves using Ludwik equation [23,25]:

$$\sigma = \sigma_y + K_1\varepsilon^{n_1} \quad (3)$$

where n_1 is the strain hardening exponent and K_1 is the strength coefficient which represents the increment in strength due to strain hardening at $\varepsilon = 1$.

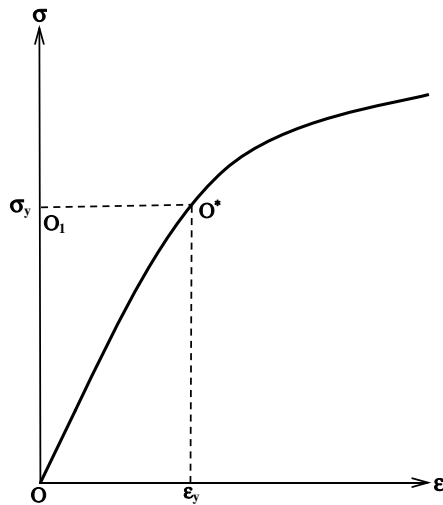
Eq. (2) has been widely used to evaluate the strain hardening exponent of materials. However, the entire true stress–true strain curve as schematically shown in Figure 3 is implied to fit in Eq. (2), including the elastic deformation stage where the Hooke’s law holds true (i.e. with the origin located at O), even though only the data between YS and UTS are used in the curve fitting. The evaluation of the strain hardening exponent based upon Eq. (3) means the exclusion of YS, equivalent to shifting the origin from O to O_1 in Figure 3. In the present study the strain hardening exponent is evaluated according to the following equation:

$$\sigma = \sigma_y + K^*(\varepsilon - \varepsilon_y)^{n^*} \quad (4)$$

where n^* , σ , ε , σ_y and ε_y are the strain hardening exponent, true stress, true strain, yield strength and yield strain of a material, respectively. K^* is the strength coefficient which reflects the increment in strength due to strain hardening corresponding to $(\varepsilon - \varepsilon_y) = 1$. Our modified Eq. (4) represents the exclusion of both yield stress and yield strain, equivalent to shifting the origin from O to O^* in Figure 3. In other words, the proposed Eq. (4) represents a relationship between the net flow stress $(\sigma - \sigma_y)$ vs. plastic train $(\varepsilon - \varepsilon_y)$ in the uniform

Table 1. Yield strength, ultimate tensile strength, hardening capacity and strain hardening exponents of the base alloy and FSWed samples of AZ31B-H24 Mg alloy tested at different strain rates

Specimen	Welding speed (mm/s)	Average strain rate (s^{-1})	YS (MPa)	UTS (MPa)	Hardening capacity	n -value	n_1 -value	n^* -value
Base alloy	–	6.0×10^{-4}	207	306	0.48	0.10	0.27	0.21
		6.7×10^{-5}	206	302	0.47	0.10	0.28	0.24
		7.0×10^{-6}	202	315	0.56	0.10	0.25	0.23
Sample IV	2	3.0×10^{-2}	99	178	0.79	0.40	1.22	0.89
		6.0×10^{-3}	96	185	0.92	0.39	1.13	0.87
		6.0×10^{-4}	100	186	0.86	0.40	1.04	0.85
		6.7×10^{-5}	102	202	0.98	0.39	0.94	0.79
		7.0×10^{-6}	90	193	1.14	0.37	0.84	0.70
Sample VI	4	3.0×10^{-2}	113	203	0.79	0.36	0.98	0.73
		6.0×10^{-3}	113	205	0.81	0.36	0.96	0.70
		6.0×10^{-4}	113	200	0.77	0.35	0.98	0.73
		6.7×10^{-5}	112	202	0.80	0.35	0.91	0.67
		7.0×10^{-6}	115	208	0.81	0.32	0.78	0.61

**Figure 3.** Schematic illustration of a true stress vs. true strain curve.

plastic deformation region, in which the elastic deformation stage or Hooke's law is no longer included in the evaluation of the strain hardening exponent.

The strain hardening exponents evaluated using Eqs. (2)–(4) are listed in Table 1. It is seen that n^* lies in-between n and n_1 , and n is smaller than n_1 and n^* , which appear to be more sensitive to the change in strain rates since they basically decrease with decreasing strain rate. FSWed samples showed much higher (about triple) strain hardening exponents compared with the base alloy, which was similar to the hardening capacity H_c value, where about twofold increase after FSW was seen in Table 1. While a slower welding speed led to a lower strength, the hardening capacity and strain hardening exponents were slightly higher.

To explain strain hardening behavior it is important to consider both grain size strengthening and dislocation hardening effects. A recent strain hardening model took into account both effects [16,26],

$$\sigma = \sigma_0 + \sigma_{HP} + \sigma_d \quad (5)$$

where σ_0 is the frictional contribution, $\sigma_{HP} = kd^{-1/2}$ is the Hall–Petch contribution and $\sigma_d = M\alpha Gb\rho^{1/2}$ is the

Taylor dislocation contribution, ρ is the dislocation density, α is a constant, M is the Taylor factor, G is the shear modulus and b is the Burgers vector.

The strain hardening of a material after yielding is related to the dislocation strain field interactions. Stress contribution due to dislocation density can be obtained by subtracting the yield stress from the total flow stress and can be written as [16]: $\rho^{1/2} \propto \sigma_d \approx \sigma - \sigma_y$. Then the applied stress necessary to deform a material is proportional to the dislocation density inside the material. An increase in the number of dislocations during a deformation process decreases the spacing among them and their interaction becomes repulsive. As the number of dislocations increases, the resistance to the dislocation movement increases and the stress required to deform the materials becomes higher with increasing deformation or cold work [10].

Based on the above discussion, the high initial dislocation density in the material created during fabrication might have contributed to the initial high and nearly constant strain hardening rate (i.e. stage II linear hardening shown in Fig. 2) of the base alloy. This suggests that much higher activation energy is required for the plastic flow due to very strong barriers to the dislocation movement [18,20]. Since stage II linear hardening is a thermal in nature, the chief mechanism could be related to the evolution of long-range stresses due to dislocation pile-ups at the grain boundary [20]. Srinivasan and Stoebe [27] reported that the presence of stage II strain hardening could also be due to the interaction of the dislocations in the primary slip system with those in an intersecting slip system. In the present study the FSWed samples did not exhibit any stage II linear hardening behavior, and their stage III with a decreasing θ occurred immediately after yielding (Fig. 2). At high temperatures and for materials with high stacking-fault energy (SFE) it is possible that stage III may limit the extent of stage II and even eliminate it as a separate stage [19]. Magnesium alloy was reported to have low SFE of about 60–78 mJ m⁻² [28]. This could be the reason for the occurrence of stage II and the delayed onset of stage III in the base alloy due to difficult cross-slip [22].

The strain hardening of a material at a higher strain hardening stage is more related to the dislocation strain field interactions. Thus the Taylor dislocation contribu-

tion $\sigma_d = M\alpha Gb\rho^{1/2}$ in Eq. (5) dominates this region. As mentioned above, after FSW, recrystallization and grain growth occurred in the SZ. This resulted in a low initial dislocation density in the FSWed samples [12]. The bigger grain size of the FSWed samples provided more space to accommodate dislocations, hence stronger strain hardening ability was observed at later stages of deformation. In this study the strain hardening exponent was evaluated in the stage III plastic deformation region, where the base alloy showed a rapid decrease in θ . Many dislocations created during cold work and stored in the base alloy may have taken part in the annihilation rather than multiplication, which might have contributed to the rapid θ decrease and the low stage III strain hardening exponent of the base alloy. Sample IV, with a lower welding speed, showed a slightly higher hardening capacity and strain hardening exponent than sample VI, as seen in Table 1. This can also be explained by the difference in the grain size between the two samples, with sample VI having a slightly smaller grain size due to the lower amount of heat input [17]. This reduction in grain size may have resulted in the reduced dislocation storage capacity in sample VI, which contributed to both the lower hardening capacity and the lower strain hardening exponent.

In summary, the flow stress of FSWed samples was lower compared with that of the base alloy. While FSW resulted in about half of the yield strength of the base alloy, the ultimate tensile strength after FSW could reach about two-thirds of that in the base alloy. This led to a higher hardening capacity of the FSWed samples, which was approximately twice that of the base alloy. After yielding, the base alloy showed a high initial and almost constant strain hardening rate, corresponding to stage II linear hardening, followed by stage III hardening of linearly decreasing hardening rate, before stage IV hardening appeared. After FSW, stage II hardening was absent and stage III hardening occurred immediately after yielding. Two modified equations, i.e. Eqs. (1) and (4), were proposed to evaluate the strain hardening capacity and exponent. The strain hardening exponent of the FSWed samples in almost all cases was about three times higher than that of the base alloy. The slower welding speed in the FSW resulted in higher hardening capacity and strain hardening exponent.

The authors would like to thank the National Sciences and Engineering Research Council of Canada (NSERC) for providing financial support. This investigation involves part of a multi-national Canada–China–USA Collaborative Research Project on the Magnesium Front End Research and Development (MFERD). D.L.C. is also grateful for the financial support by the Premier's Research Excellence Award (PREA) and Ryerson Research Chair (RRC) programs. The authors would like to thank A. Machin, Q. Li, J. Amankrah, R. Churaman and M. Guerin for their assistance in the experiments.

- [1] A. Weisheit, R. Galun, B.L. Mordike, *Weld. J.* 77 (1998) 149.
- [2] W.M. Thomas, E.D. Nicholas, J.C. Needham, M.G. Church, P. Templesmith, C.J. Dawes, GB patent application no. 9125978.8 (1991).
- [3] R.S. Mishra, Z.Y. Ma, *Mater. Sci. Eng. R* 50 (2005) 1.
- [4] S.H.C. Park, Y.S. Sato, H. Kokawa, *Scripta Mater.* 49 (2003) 161.
- [5] W.B. Lee, Y.M. Yeon, S.B. Jung, *Mater. Sci. Technol.* 19 (2003) 785.
- [6] T. Nagasawa, M. Otsuka, T. Yokota, T. Ueki, in: H.I. Kaplan, J. Hryn, B. Clow (Eds.), *Magnesium Technology*, TMS, Warrendale, PA, 2000, p. 383.
- [7] S.H.C. Park, Y.S. Sato, H. Kokawa, *J. Mater. Sci.* 38 (2003) 4379.
- [8] S. Lim, S. Kim, C.G. Lee, C.D. Yim, S.J. Kim, *Metall. Mater. Trans. A* 36 (2005) 1609.
- [9] W.B. Lee, J.W. Kim, Y.M. Yeon, S.B. Jung, *Mater. Trans.* 44 (2003) 917.
- [10] W.D. Callister Jr., *Materials Science and Engineering – An Introduction*, seventh ed., John Wiley & Sons, New York, 2007.
- [11] X.H. Chen, L. Lu, *Scripta Mater.* 57 (2007) 133.
- [12] I. Kovács, N.Q. Chinh, E. Kovács-Csetényi, *Phys. Stat. Sol. (a)* 194 (2002) 3.
- [13] T.L. Johnston, C.E. Feltner, *Metall. Trans.* 1 (1970) 1161.
- [14] G.Y. Sha, Y.B. Xu, T. Yu, X.L. Zhang, E.H. Han, L. Liu, *Trans. Mater. Heat Treat.* 27 (2006) 77.
- [15] L. Jiang, J.J. Jonas, A.A. Luo, A.K. Sachdev, S. Godet, *Scripta Mater.* 54 (2006) 771.
- [16] J.A. del Valle, F. Carreno, O.A. Ruano, *Acta Mater.* 54 (2006) 4247.
- [17] N. Afrin, D.L. Chen, X. Cao, M. Jahazi, *Mater. Sci. Eng. A*, in press. doi:10.1016/j.msea.03.018.
- [18] J. Luo, Z. Mei, W. Tian, Z. Wang, *Mater. Sci. Eng. A* 441 (2006) 282.
- [19] U.F. Kocks, H. Mecking, *Prog. Mater. Sci.* 48 (2003) 171.
- [20] G.E. Dieter, *Mechanical Metallurgy*, third ed., McGraw-Hill, Boston, MA, 1986.
- [21] W.F. Hosford, *Mechanical Behavior of Materials*, Cambridge University Press, New York, 2005.
- [22] R.W. Hertzberg, *Deformation and Fracture Mechanics of Engineering Materials*, fourth ed., John Wiley & Sons, New York, 1996.
- [23] L. Ratke, P.I. Welch, in: 13th Biennial Congress – International Deep Drawing Research Group: Efficiency in Sheet Metal Forming, Melbourne, Australia, 1984, pp. 427–435.
- [24] J.H. Hollomon, *Trans. AIME* 162 (1945) 268.
- [25] P. Ludwik, *Elemente der Technologischen Mechanik*, Springer-Verlag, Berlin, 1909.
- [26] J.A. del Valle, O.A. Ruano, *Scripta Mater.* 55 (2006) 775.
- [27] M. Srinivasan, T.G. Stoebe, *J. Mater. Sci.* 9 (1974) 121.
- [28] M.M. Avedesian, H. Baker (Eds.), *Magnesium and Magnesium alloys*, ASM Specialty Handbook, ASM International, Materials Park, OH, 1999.